Article:
Luo, Y., Zhang, L., Chen, C. et al. (2 more authors) (2024) Real-Time Diagnosis of Open Circuit Faults in Three-Phase Voltage Source Inverters. IEEE Transactions on Power Electronics, 39 (6). pp. 7572-7585. ISSN 0885-8993

https://doi.org/10.1109/tpel.2024.3371452

Real-time Diagnosis of Open Circuit Faults in Three-Phase Voltage Source Inverters

Yu Luo, Li Zhang, Senior Member, IEEE, Chunyang Chen, Kang Li, Senior Member, IEEE, and Kaidi Li

***Abstract*—This paper investigates the real-time diagnosis of single and double open circuit faults (OCFs) in three-phase voltage source inverters (VSI). The method analyzes the phase current waveforms continuously in real-time, and abnormal patterns of the current waves due to the corresponding switch OCFs are extracted to define as the fault detection waveforms (FDW). The current values of the FDWs are analyzed and a new scheme is developed to distinguish current waveform patterns from that of normal to unbalance loads situation and switch OCFs. The scheme detects the starting zero crossing point first and then checks the magnitudes of the FDW. Periodic detections are applied to identify whether the collected data samples are within the FDW current range. The OCFs of the inverter switches are identified by counting the fault points within the predicted samplings of FDWs. The method has been verified through both simulations and experiments. The results confirm the effectiveness of the proposed scheme.**

***Index Terms*—voltage source inverter, open circuit fault, fault diagnosis, unbalance load, current samples.**

I. Introduction

THREE-phase voltage-source inverters (VSIs) are capable of converting electrical energy from DC power sources, including batteries, solar cells, or fuel cells, into AC voltages with flexible frequencies and amplitudes. Due to their high efficiency and control flexibility, three-phase voltage-source inverters (VSIs) play a vital role in modern industrial and energy sectors[1], [2]. The power semiconductor switch devices commonly employed in three-phase voltage-source inverters (VSIs) are metal-oxide-semiconductor field-effect transistors (MOSFETs) and insulated gate bipolar transistors (IGBTs) [3], [4]. Recent advancements in power device manufacturing have led to the widespread utilization of wide bandgap materials such as silicon carbide (SiC) or gallium nitride (GaN) in inverters[5], [6]. Switch failures are a prevalent issue in three-phase inverters, which rely on power semiconductor switch devices that are relatively delicate and subject to high voltage stress[7], [8].

Such switches in inverters are susceptible to short-circuit and open-circuit faults. Short-circuit faults are highly destructive, causing high current flow, but are typically detected by standard protection systems such as fuses and circuit breakers, resulting in an immediate shutdown of the inverter [9], [10]. In contrast, implementing open-circuit fault (OCF) protection requires additional circuits and equipment, with an increase in manufacturing cost and complexity of the inverter. Consequently, OCF protection is not typically included as a standard offer in industrial applications[11], [12]. However, open-circuit faults can also lead to drive circuit and load failures, and other secondary faults. Fast and accurate methods for diagnosing open-circuit faults are therefore crucial to prevent faults propagating to other parts of the system [13], [14]. OCF diagnosis is also essential for preventing prolonged operation with faulty switches, which can result in distorted output waveforms, abnormal load operation, and overheating [15].

In the voltage-based methods, the actual voltage can be obtained from additions to the functional circuitry or from dedicated voltage sensors. Simple hardware circuits as described in references [16] and [17] can achieve diagnosis in a very short period of time. On the other hand, to reduce the need for extra hardware, a mixed logical-dynamical or switch function model can be established[18], [19], [20], [21]. In [18], a voltage envelope line is generated by the proposed voltage envelope function. By comparing the preprocessed diagnostic eigenvalue and the voltage envelope, open-circuit faults can be located precisely. This is a highly reliable method but is limited to diagnosing a single switch open circuit fault. As shown in [19], faults can be quickly diagnosed from the ratio, the difference, and the arithmetic values, of the two line voltages. The results show that the proposed method is robust to load variation and immune to certain load OCFs, but the robustness and reliability need to be improved when the load is a motor or motors. In [20], faults are defined by analysing the voltage patterns in the Alpha-Beta plane. The proposed method can identify all possible types of switch open-circuit faults in a three-phase inverter and locate the faulty switches without complex calculations or additional hardware. The drawback of this method is its limited adaptability to various loads, exhibiting poor robustness. In[21], the voltage between the midpoints of the DC side and AC side is utilized for detecting open circuit faults and determining the upper and lower positions of the faulty switch. The diagnostic process is fast but again is limited to diagnosing single switch open circuit faults.

The open circuit fault diagnosis method based on current features exhibits high sensitivity, real-time capability, reliability, and a certain level of robustness, enabling effective detection and diagnosis of open circuit faults in three-phase

Manuscript received XX XX, 2023. This work was supported by the Fundamental Research Funds for the Central Universities of Central South University (2018zzts164).

Yu Luo, Chunyang Chen are with the School of Traffic and Transportation Engineering, Central South University, Changsha, 410075, China. Li Zhang and Kang Li are with the School of Electrical Engineering,University of Leeds, Leeds, UK. Kaidi Li is with Shenzhen Metro Group, Shenzhen, 518000, China. (e-mail: 174201007@csu.edu.cn,cychen999@csu.edu.cn,Yingchun Shi@csu.edu.cn, L.Zhang@leeds.ac.uk, K.Li1@leeds.ac.uk, likaidi@shenzhenmc.com).

inverters. In [22], the zero voltage vector sampling method is used to sample current during the two zero voltage vectors and reconstruct the three-phase currents. These are used to generate the diagnostic variables that can detect and locate the faulty power switches. The method has a good and fast diagnostic response to open circuit faults (OCFs), but it is very poor at handling load variations. It relies heavily on the accuracy of the basic model parameters. In [23], the sum of the absolute values of the normalized phase currents is calculated, and the current zero-crossing detection method is used to avoid the influence of current distortion caused by the transient condition; the fault detection signal is built to precisely localize the faulty switches. The method has limited capability in detecting all the fault types and also lacks robustness to load variations. In [24], the open-circuit faults of the inverter lead to output phase current distortion. Different types of faults have different space trajectories, and the corresponding fault feature is located by the direction vector and center-of-mass coordinate. The OCFs are diagnosised by the fault feature. This method is effective in handling certain load variation scenarios and is capable of handling multiple fault conditions. However, it does not take into account open circuit faults (OCFs) in cases of load imbalance. In [25], the three-phase current signal is de-composed into the trend, seasonal, and remainder components through the simplified seasonal trend decomposition algorithm. The thresholds of characteristic quantities are set, and a diagnosis algorithm is designed to detect the OCFs. The complexity of the algorithms involved demands an appreciable amount of diagnostic time. In [26], A unique faulty characteristics of diagnosis variables for each fault are extracted by combining two kinds of diagnosis variables, line voltage deviations and phase voltage deviations to distinguish the fault. This method exhibits a very fast response speed in fault diagnosis; however, it can only handle single open circuit faults (OCFs). Additionally, it has the drawbacks of poor capability to handle load variations with low reliability.

Over the past few years, there has been a considerable amount of research using model-based fault diagnosis for inverter drive systems. In [27], a method based on calculated average bridge arm pole-to-pole voltages and error-adaptive thresholds is presented for diagnosing the OCFs. This method demonstrates good diagnostic capabilities for various faults; however, it has certain computational requirements and lacks consideration for different load scenarios. In [28], a new fault feature extraction method is proposed by the trend relationship of adjacent fold lines for data curve. It can be used to extract the fault feature and it is not affected by asymmetric interference. The fault diagnosis time of this method is short; however, it is limited in terms of the number of fault types it can handle, and it requires high computational capability. In [29], based on the vector decomposition principle and voltage-second balancing theory, the output phase voltage model is established considering neutral point voltage imbalance and time-offset injection. The faults can be located by building two suspected phase voltage models to approximate the real system. The fault diagnosis algorithm of this method is complex, and there is room for improvement in its capability to handle load variations.

Intelligent technologies have become a hot research topic in fault diagnosis for three-phase inverters, as they possess characteristics such as automation, data-driven analysis, the ability to diagnose multiple fault types, self-learning and adaptability, as well as remote monitoring and management. In [30], transient time-domain sequence data under different faults are analyzed, and raw signals are taken as fault representations without manually selecting feature extraction methods. An end-to-end method based on an improved convolutional neural network model has been proposed for inverter fault diagnosis. The computational requirements of this method are moderate; however, it can only handle single switch open circuit faults (OCFs) in scenarios with minimal load variations. In [31], an extreme learning machine model is trained by the data from the source system to form an initial diagnostic model. After that, a model adaption process is designed to adjust the model parameters by minimizing the distribution divergence between the data from the source and target systems. This method is capable of handling scenarios with varying load conditions and exhibits strong transfer learning capabilities, albeit requiring a certain level of computational resources. In [32], parallel structural stacked LSTM networks are constructed, the attention mechanism is applied to weight these features adaptively and the fault is identified by features that integrate multiple sources of information. If supported by high computational power, this method can effectively diagnose faults. However, it does not take into account scenarios with load variations.

Motivated by the aforementioned techniques, this paper presents a real-time, cost-effective method for open-circuit fault (OCF) diagnosis in three-phase voltage source inverters (VSIs). The method identifies the feature changes of the current waveforms, which is defined the fault detection waveforms (FDW), when switch OCF occurs. It can locate the faulty switches through statistical analysis of current half-waves in each phase of the VSI. The scheme analyses the distinctive fault characteristics of FDW to identify the conditions from normal to unbalanced load and switch OCFs. The procedure developed employs statistical analysis to detect the OCFs of the inverter switches by counting fault points within the FDWs. The proposed method offers notable advantages over existing approaches, including fast fault detection, precise fault localization, low calculation burden and high robustness. It enables real-time diagnosis without necessitating additional hardware, leveraging the existing equipment employed for regular operation. The method has the potential in finding wide-ranging applications in traction drive systems, as well as general mechanical drive systems.

This paper focuses on highlighting advancements, especially in the analysis of current variations during open-circuit faults (OCFs). This becomes crucial when considering the significant reduction in switch currents caused by double switch open-circuit faults on the inverter's same side. This refined analysis enhances accuracy in open-circuit fault current assessment and effectively addresses the issue of misdiagnosis seen in previous current-centric diagnostic methods. Furthermore, the proposed current normalization technique introduces a transformative concept, the imbalance factor, beyond accounting for current

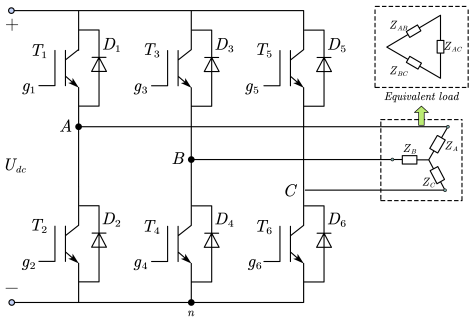

Fig. 1. Topology of three phase inverter

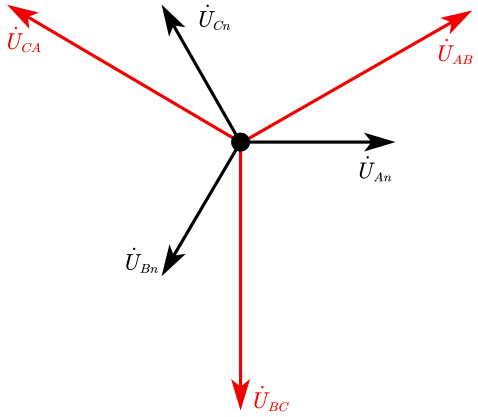

Fig. 2. Voltage vectors generated by a three-phase inverter

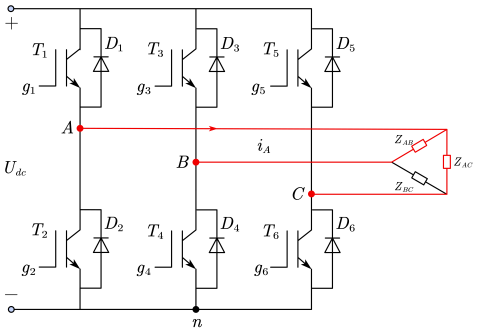

Fig. 3. Path of phase A current flow in three-phase VSI

amplitude changes. This innovative addition helps mitigate the disruptive effects of load fluctuations on open-circuit fault diagnosis. This adaptable normalization approach significantly boosts the flexibility and effectiveness of fault diagnosis methods, especially in dynamic load conditions. In conclusion, the method's effectiveness is evident in its ability to handle minor load imbalances and sudden fluctuations adeptly.This robustness enhances the practical value and reliability of the method.

The remaining sections of this paper are organized as follows. Section II introduces the inverter topology and basic mathematical modeling of the VSI, and different fault scenarios. Section III analyzes the fault detection waveforms for each switch, the variations of fault current values during OCFs in the inverter, and the impact of unbalanced loads. In Section IV, the diagnosis method based on fault detection waveforms of current values is elaborated, including fault detection and clear misdiagnoses. In Section V, the proposed fault diagnosis method is validated through MATLAB Simulink simulations based on a model of a train air conditioning inverter. The experimental platform used to validate the proposed diagnostic method is introduced in Section VI, and the experimental results confirm the effectiveness and feasibility of the proposed method in comparison with different diagnosis methods. Finally, conclusions are provided in Section VII.

II. VSI CURRENT AND FAULT CLASSIFICATION

A. Three-phase VSI load impedance and transformation

Fig. 1 depicts a typical three-phase two-level voltage source inverter consisting of three phase legs with six semiconductor switches (T_1-T_6) and their corresponding six freewheeling diodes (D_1-D_6). In engineering applications, a load connected to the inverter such as an induction motor is usually star-connected with its three stator windings having the same number of distributed coils with identical number of turns. Thus the load phase impedance values are equal and well-balanced i.e., Z_a=Z_b=Z_c=Z_Y. As illustrated in Fig. 1, a star-connected load can be transformed to its equivalent delta-connected form. The phase impedance, in this case, can be expressed by the following equations.

$$\begin{cases} Z_{AB} = Z_A + Z_B + \frac{Z_A Z_B}{Z_C} \\ Z_{BC} = Z_B + Z_C + \frac{Z_B Z_C}{Z_A} \\ Z_{AC} = Z_A + Z_C + \frac{Z_A Z_C}{Z_B} \end{cases} \tag{1}$$

With the three-phase load having the same impedance, the corresponding equivalent impedances from (1) are equal, Z_{AB}=Z_{BC}=Z_{AC}=Z_Δ. The VSI supplies a three-phase switch mode voltage which synthesizes three-phase sinusoidal voltage to the load with equal amplitude and phase angle difference of 120 degrees between each phase, the phasor expressions of the voltages are given as

$$\begin{cases} \dot{U}_{An} = U_m e^{j\omega t} \\ \dot{U}_{Bn} = U_m e^{j\omega t - 2\pi/3} \\ \dot{U}_{Cn} = U_m e^{j\omega t - 4\pi/3} \end{cases} \tag{2}$$

where U_m is the magnitude of the phase voltage. Fig. 2 illustrates the vector relationship between the phase and line-line voltages. The line voltages of the three-phase inverter can be written as

$$\begin{cases} \dot{U}_{AB} = \sqrt{3} U_m e^{j\omega t + \pi/6} \\ \dot{U}_{BC} = \sqrt{3} U_m e^{j\omega t - \pi/2} \\ \dot{U}_{CA} = \sqrt{3} U_m e^{j\omega t + 5\pi/6} \end{cases} \tag{3}$$

Consider six switches in a VSI shown in Fig. 3, when T_1,T_4 and T_6 are turned on, according to Kirchhoff's current law, the current flowing through phase A is the sum of the current generated by the line voltage U_{AB} applied to the load Z_{AB} and that generated by the line voltage U_{AC} applied to the load Z_{AC}. Fig. 3 illustrates the path of the current flow of phase A under this condition. Therefore the equation for calculating the current of phase A is given by

$$\dot{I}_A = \frac{\dot{U}_{AB}}{Z_{AB}} + \frac{\dot{U}_{AC}}{Z_{AC}} \tag{4}$$

B. Fault cases for a three-phase VSI

In practice, single-switch or double-switch open-circuit faults (OCFs) are the most common in three-phase VSIs, TABLE I lists 22 types of inverter operating conditions, including one normal operation and 21 OCF conditions. The fault conditions are divided into four categories. Case I: Single OCF. Case II: Two OCFs in the same inverter leg. Case III: Two OCFs occurring on two different inverter phase legs and on different sides of a three-phase VSI. Case VI: Two OCFs on two different inverter phase legs at the same sides.

TABLE I
FAULT CLASSIFICATION AND LABELS

Case	Faulty switch	Case	Faulty switch
Nomal	No fault	III	T_1, T_6
I	T_1		T_2, T_3
	T_2		T_3, T_6
	T_3		T_2, T_5
	T_4		T_4, T_5
	T_5	IV	T_1, T_3
	T_6		T_1, T_5
II	T_1, T_2		T_3, T_5
	T_3, T_4		T_2, T_4
	T_5, T_6		T_2, T_6
III	T_1, T_4		T_4, T_6

III. FAULT CURRENT ANALYSIS

A. Fault detection waveform (FDW) for each switch

The operation of each inverter phase can be divided into two states, inserted state and bypassed state, based on the gate signals applied to the corresponding switches. Taking phase A as an example, when T_1=1 and T_2= 0, phase A is in the inserted state (1 indicates the switch is on, while 0 indicates the switch is off). Similarly, when T_1=0 and T_2=1, phase A is in the bypassed state. To describe these two states clearly, the switching function S_A can be defined as

$$S_A = \begin{cases} 1 \ T_1 = 1 \& T_2 = 0 \ \ (inserted) \\ 0 \ T_1 = 0 \& T_2 = 1 \ \ (bypassed) \end{cases} \tag{5}$$

This is also applied to phases B and C.

When an OCF occurs in a three-phase VSI, it results in a change in the current flowing through the faulty switch. Fig. 4 illustrates the effect of an OCF occuring in switch T_1 on the phase A current. Fig. 4(a) shows the operation mode when $i_A > 0$, S_A = 1 and T_1 has OCF.

Under the normal condition, there may be a current flowing from the positive DC terminal, like i_c through switch T_1 to AC terminal A. However, since T_1 has OCF, i_c will not pass through T_1 to phase A. The current i_A is drastically reduced and not equal to i_c.

Fig. 4(b) shows the situation when $i_A > 0$, S_A = 0 and T_1 OCF. Under the nomal condition, S_A= 0 means T_1 is bypassed but there is still a current path through T_2 or its freewheeling diode D_2. The current is either a reactive current or from the other parts of the circuit such as phases B and C. So when T_1 has OCF, i_A is not affected, since the current flowing path is the freewheeling diode D_2.

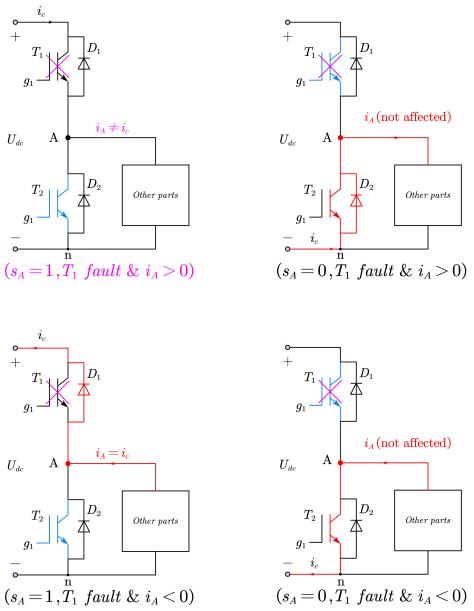

Fig. 4. the current analysis of T_1 fault

TABLE II
THE FDW OF SIX SWITCHES

Switch	Phase	Halfwave	Switch	Phase	Halfwave
T_1	A	+	T_2	A	–
T_3	B	+	T_4	B	–
T_5	C	+	T_6	C	–

Fig. 4(c) shows another situation when $i_A < 0$, S_A = 1 and T_1 has OCF. In this case under the normal condition, i_A is negative flowing from A to positive terminal of DC source through its freewheeling diode D_1. Thus the flow path of i_A is unaffected.

Fig. 4(d) depicts another scenario, switch T_1 is bypassed even though it has OCF, there has no effect on the magnitude of current i_A.

To summarize from the above , when an OCF occuring on switch T_1, i_A will be drastically reduced only in the situation shown in Fig. 4 (a), when its current is positive. Therefore, to detect OCF on T_1, we need to monitor the behavior of the phase A current during the positive half-cycle, which is defined as the fault detection waveform (FDW) for T_1.

The same analysis as above can be applied to the other switches for detecting their OCF conditions. Table 1 describes FDWs for the six switches. For switches T_3 and T_5, their FDW are the positive half-cycle wave of phases B and C, respectively. The FDWs of switches T_2, T_4, and T_6 are the negative half-cycle period of phases A, B, and C currents respectively.

B. Current analysis under different fault cases

Taking switch T_1 as an example, based on the fault classification listed in Table 1, the possible operation scenarios for a VSI include the following three types

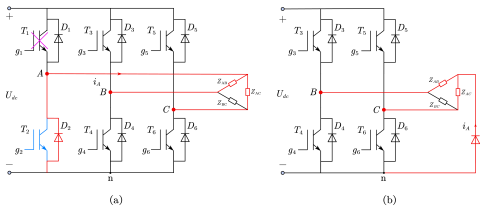

Fig. 5. Phase A current circuit when T_1 OCF (S_A=0, $i_A > 0$)

(1) The inverter is in normal operation condition.

(2) Six separate cases all involving T_1 having OCF(see Table.1),these are Case I (T_1 OCF), these are Case I (T_1 OCF) , Case II (T_1 and T_2 OCF), Case III (T_1 and T_4, or T_1 and T_6 OCF), Case IV (T_1 and T_3 or T_1 and T_5 OCF).

(3) T_1 is not faulty but the other five switches having OCF separately.

For (1) above, phase A current is a normal sinusoidal. However for situation (2), Case I, phase A current i_A is significantly reduced compared to that under normal condition with the same load as shown in Figs.4 (a) and (b).

Fig. 5 shows current i_A flowing path when T_1 has OCF. The current originates from the other part of the inverter and passes the on-state switch T_2 or the freewheeling diode D_2. Assuming the three-phase load is star (Y) connected as shown in Fig. 5(a), it can be transformed to the equivalent delta (Δ) load for analysis as shown in Fig. 5(b), using equation (1). This is primarily to simplify the analysis for better understanding of the relationships between the OCF current and normal current.

Fig. 5(b) shows the equivalent circuit of Fig. 5(a). According to Kirchhoff's current law, the output current of phase A, shown in Fig. 5(b), is the sum of the current generated by V_{Bn} applied on the Z_{AB} load and that generated by V_{Cn} applied on the Z_{AC} load, namely

$$\dot{I}_{A\_fault} = \frac{\dot{U}_{Bn}}{Z_{AB}} + \frac{\dot{U}_{Cn}}{Z_{AC}} \tag{6}$$

When the load is balanced, combining equations (1)-(4) and (6), we can express the magnitude of current under normal condition as

$$\left|\dot{I}_A\right| = \left|\frac{\dot{U}_{AB} + \dot{U}_{BC}}{Z_\Delta}\right| = 3\frac{U_m}{Z_\Delta} \tag{7}$$

and that when T_1 has OCF as

$$\left|\dot{I}_{A\_fault}\right| = \left|\frac{\dot{U}_{Bn} + \dot{U}_{Bn}}{Z_\Delta}\right| = \frac{U_m}{Z_\Delta} \tag{8}$$

The ratio of the fault current magnitude to the magnitude of current under normal condition can be expressed as follows.

$$R = \frac{\left|\dot{I}_{A\_fault}\right|}{\left|\dot{I}_A\right|} = \frac{1}{3} \tag{9}$$

Thus when T_1 is in OCF condition, the maximum value of i_A within FDW will be less than one-third of the magnitude of the current under normal conditions. This can be used to diagnose and locate the OCFs in a three phase VSI.

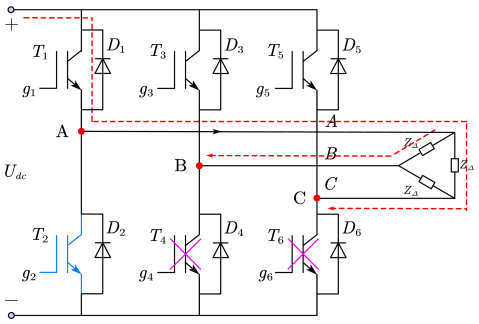

Fig. 6. Phase A current when T_4 and T_6 faulty (i_A)

TABLE III
SIX CASES OF TWO SWITCHES HAVING OCF

Affected switch	OCF switches	Affected switch	OCF switches
T_1	T_4T_6	T_2	T_3T_5
T_3	T_2T_6	T_4	T_1T_5
T_5	T_2T_4	T_6	T_1T_3

The above analysis is for fault scenarios (2), Case I, while for fault mode (2), Cases II, III, and VI, these are for the scenarios that one of the remaining five switches have OCF with T_1. Fig. 5(a) shows that in these five cases, the effect on the FDW current of T_1 flowing path is negligible. The current will be still less than 1/3 of its normal value. Equation 9 is also applicable to mode (2), Case II, Case III, and Case VI.

For scenarios (3), when T_1 is not faulty, during the FDW of T_1, the current i_A is the sum of the current generated by voltage U_{AB} applied on load Z_{AB} and the current generated by voltage U_{BC} applied on load Z_{AC}. However, when both T_4 and T_6 are in OCF condition simultaneously, no current will pass through phase A. The current value characteristic is similar to the scenarios when T_1 in OCF condition, the current i_A decreases significantly.

Fig. 6 depicts the current flow path of scenario (3) case T_4 and T_6 have OCFs simultaneously. The dashed line in the diagram indicates the normal i_A flowing path. However due to both T_4 and T_6 are in OCF condition, this path cannot be established, leading to i_A current significantly decreased. Consequently, a zero current mode similar to that due to T_1 OCF is formed.

This implies that when we apply the current ratio of less than 1/3 as the fault detection criterion for detecting a single switch having OCF in a three-phase VSI, we must take into account the fault conditions involving two switches from two different phase legs and at the same sides being simultaneously faulty and exclude them.

TABLE III displays the six cases when two switches are in OCF simultaneously leading to misdiagnosis respectively.

C. Fault Diagnosis Under Unbalanced Load Current

1) Unbalanced loads: The above discussion assumes operating conditions where switch OCFs occur with well-balanced loads connected to the VSIs. Abnormal conditions causing load imbalance in practical applications may include: (a) Circuit aging: very severe insulation deterioration and conductor

oxidation, in a load motor, could unbalance the load phase impedances, at a level that would affect diagnosis of inverter faults. This effect would probably be much too severe to permit continued operation. (For example, it could possibly present a fire risk.) (b) Partial phase circuits shorting in three-phase equipment, e.g. from shorting turns in machine windings. (c) Load open circuit faults: One phase of the load becomes open circuited, resulting in a disruption to the current flow. (d) Load short circuit faults: A load experiencing a phase to ground or phase to phase short circuit would generally have severely abnormal current waveforms.

Note that a severe current imbalance in a three-phase inverter system, such as in cases (c) and (d), or arising in the inverter, can result in motor vibration severe enough to damage it and other equipment. Such situations would require the complete drive system to be switched off. Modest imbalance can also occur in loads that are not inherently balanced but where a useful attempt at equal partitioning has been made. In this work, only minor load imbalance faults are considered, where the system can still operate without the whole system being switched off. Equipment losses and electromagnetic interference may remain tolerable, but importantly the accurate detection and diagnosis of inverter switch OCFs may be affected. Hence it is clearly worth considering ways of mitigating the effect of moderate load imbalances on the accuracy of diagnosis of inverter faults.

As described in Section II, for each of the six switches in a VSI, their OCF corresponds to a unique current FDW and the magnitude of this FDW is noted as $I_{m\_T_p}$, (p = 1-6). For example $I_{m\_T_1}$ stands for the magnitude of FDW for switch T_1. For accurate detection of switch OCF, a factor, $K_{unbalance}$ is defined as an indicator for evaluating the level of three-phase current imbalance. It is given as

$$K_{unbalance} = \frac{1}{6}\sum \frac{\left|I_{avg} - I_{m\_T_p}\right|}{I_{avg}} \tag{10}$$

where I_{avg} is the mean average of six current FDW magnitudes, defined as

$$I_{avg} = \frac{1}{6}\sum_{p=1}^{6}\left|I_{m\_T_p}\right| \tag{11}$$

During normal operation, $K_{unbalance}$ is small approaching zero, but a high value of $K_{unbalance}$ indicates a severe imbalance in the three-phase load. Simulation studies of all OCFs listed in TABLE I have shown that it is adequate to set a threshold value of 0.1 for $K_{unbalance}$ to distinguish imbalanced phase current caused by either switch OCFs or load faults. When $K_{unbalance} > 0.1$, a switch OCF may have occurred, and the detection procedure can be triggered. If $K_{unbalance} < 0.1$, it implies the load has minor faults.

In the previous exposition, the ratio of fault current magnitude to current magnitude of a three-phase VSI under normal balanced load condition was described. Similarly, combining equations (4) and (6), the ratio under unbalanced load conditions can be obtained as

$$R_{unbalance} = \left|\frac{\dot{U}_{Bn}}{Z_{AB}} + \frac{\dot{U}_{Cn}}{Z_{AC}}\right| \Big/ \left|\frac{\dot{U}_{AB}}{Z_{AB}} + \frac{\dot{U}_{AC}}{Z_{AC}}\right| \tag{12}$$

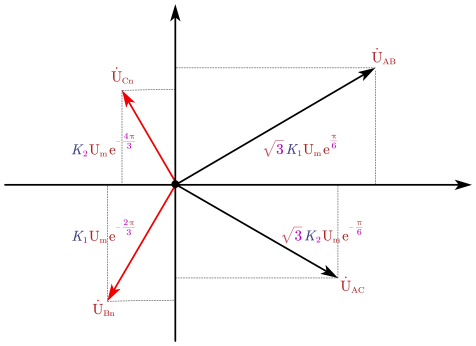

Fig. 7. The numerator and denominator vectors of $R_{unbalance}$

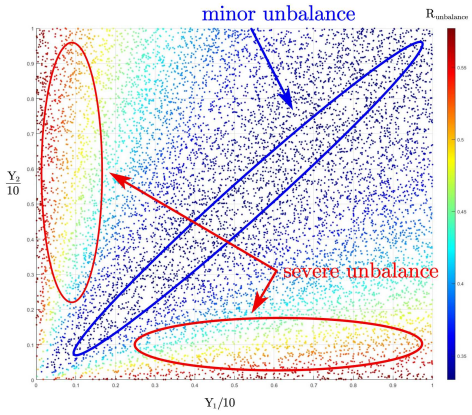

Fig. 8. Numerical distribution plot of $R_{unbalance}$ (Y_1, Y_2)

In the equation, by setting Y_1=1/Z_{AB}, Y_2=1/Z_{AC}, the numerator and denominator of Equation 12 are the magnitudes of two vectors. Fig. 7 illustrates the these vectors. By performing Cartesian coordinate decomposition and taking the magnitudes of them, we can obtain

$$R_{unbalance} = \sqrt{\frac{(Y_1+Y_2)^2 + 3(Y_1-Y_2)^2}{9(Y_1+Y_2)^2 + 3(Y_1-Y_2)^2}} \tag{13}$$

To analyze the relationship between $R_{unbalance}$ and Y_1 and Y_2, let the Y_1 and Y_2 vary in the range of 0-10. When the range of variation is 0-1 it indicates an increase in impedance, similar to the scenario(a) for circuit aging. Y_1=Y_2=1 corresponds to a standard reference loads. The variation from 1-10 corresponds to a decrease in impedance, similar to the scenario (b) internal component short circuit.

Fig. 8 shows plots of the distribution of $R_{unbalance}$ values as Y_1 and Y_2 vary. For values of $R_{unbalance}$ clustered around 0.33, the ratio of Y_1 to Y_2 is close to 1 which indicates a small imbalance. As the imbalance increasing, the ratio of Y_1 to Y_2 deviates from the line with a slope of 1, the $R_{unbalance}$ ratio exceeds 1/3. In the extremely severe unbalanced condition, the $R_{unbalance}$ even reaches up to 0.58. In summary, in minor imbalanced condition, the ratio of fault current magnitude to the magnitude of current with OCFs remains limited within a range of 1/3. The same current value characteristics also apply to the scenario of minor load imbalance.

2) Current normalization for low load cases: A three-phase inverter can be used in many areas, some examples of its application are given as follows: (a) Home appliances such as air conditioners combined with home battery energy storage systems. The three-phase inverters can convert stored DC energy into AC power for driving air conditioners or supplying other household equipment. (b) Electric vehicles for road and rail transportations. Inverters are used to convert the DC battery power to AC form to drive the electric motors pulling electric vehicles and AC tractions. (c) Industrial applications, Inverters are used in industrial machinery, such as motor controllers and variable frequency drives, to control the speed and direction of the machine tools, pumps and cooling fans etc.

Among the the aforementioned applications, (a) gives relatively low load changes. However, applications in (b) and (c) areas often present higher levels of load variations. When a motor drive powered by an inverter is running at a light or no load condition, the current drawn by the three-phase inverter decreases sharply, and can be typically as low as between 5%-10% of the rated value. Under these condition, if the rated current is still taken as the reference value for current measurement normalization as

$$I_{sample} = \frac{I_{measuremrnt}}{I_{ref}} \tag{14}$$

the resultant ratio may become less than 1/3, similar to that of an OCF current ratio, hence causing misdiagnose. Therefore, under low or no load conditions it is necessary to normalize the sampled current using a formulae different to (14), namely re-normalize the measured values of the inverter as

$$I_{sample\_T_{\rm p}} = \frac{I_{sample}}{I_{{\rm m}\_T_p}} I_{ref} \tag{15}$$

where $I_{measurement}$ is the measured value of the current, I_{ref} is the $\sqrt{3}$ times rated current of the system. Equation (14) is the normalization for normal condition, Equation (15) is the re-normalization when the measured current changed significantly due to load reduction. For operation conditions where the load varies greatly, the balance factor of the three-phase inverter load remains basically unchanged, and $K_{unbalance}$ is lower than the threshold 0.1. In this case operating the re-normalization (equ.15) can prevent the misdiagnoses of OCF under low load situation.

IV. FAULT DIAGNOSIS

A. Location of FDW

As discussed early when an OCF occurs in a switch or switches of a VSI, according to Equations (9), (13), (14) and (15), the current values evaluated according to FDW after normalization are lower than 1/3. So it is crucial to locate the FDWs of each switch for identifying whether the related switch has OCF.

Fig. 9 illustrates the FDW of T_1, there are two points important to identify whether OCF occurs; the starting point and the peak point. The former is a zero crossing point that indicates the samples after this point enter the FDW of T_1. The peak point is the one having the highest magnitude amongst

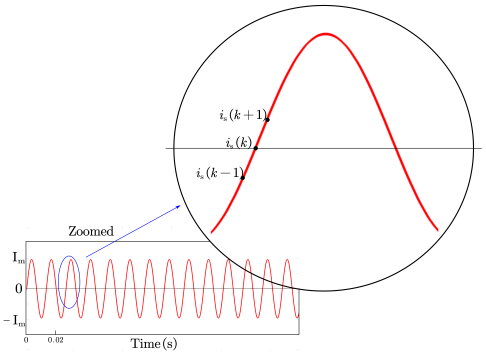

Fig. 9. The FDW zero crossing of T_1

TABLE IV
FAULT DETECTION SAMPLES FOR SIX SWITCH

Switch	Number range	Switch	Number range
T_1	[0 $N_0/2$]	T_2	[$N_0/2$ N_0]
T_3	[$N_0/3$ $5N_0/6$]	T_4	[$5N_0/6$ $4N_0/3$]
T_5	[$2N_0/3$ $7N_0/6$]	T_6	[0 $2N_0/3$]

samples of FDW, and it is noted as $I_{m\_T_1}$. The criterion for zero crossing point k can be identified as

$$\begin{cases} i_{z(k)} > 0 \\ i_{z(k)} - i_{z(k-1)} > 0 \\ i_{z(k-2)} < 0 \end{cases} \tag{16}$$

Among the three current samples ($i_z(k)$, $i_z(k-1)$, and $i_z(k-2)$ at k, k-1 and k-2 points, the one having the smallest absolute value is the starting point.

Taking switch T_1 having OCF as an example, assuming that the starting point is detected, every sample after one cycle number will be the starting point of FDW. The cycle number N_0 is defined as

$$N_0 = T_0 \times f_0 \tag{17}$$

where T_0 is the period of the inverter current, and f_0 is the sampling frequency of the current sensor.

After locating the starting point, the measured current samples are numerically labelled from 0 to $2N_0$. When the number exceeds $2N_0$ it is reset to 0 and the counting is resumed. For T_1 having OCF, every current samples from 0 to N_0/2 are within the FDW range. Due to the phase difference of 120 degrees between the three-phase currents, the starting point of T_1 can be used to obtain the fault detection samples of the six switches. TABLE IV shows the number for each switch. After locating the FDWs, we evaluate the magnitudes of six switches' $I_{m\_T_p}$ (p=1-6) which are the middle point of the FDWs, Take switch T_1 as example

$$\mathrm{I}_{\mathrm{m}\_T_1} = I_{N_0/4} \tag{18}$$

The same calculation is applied to the other five switches. Therefore the time taken for $K_{unbalance}$ for evaluating all six magnitudes is 5/6 T_0.

B. Fault diagnosis method

Under normal operations, only a small portion of current values within FDW, their ratios to the magnitude being less than 1/3. However, when the corresponding switch experiences an OCF, almost all the current samples within FDW have their ratios below 1/3. The number counting N_C for the faulty samples is defined as

$$N_C = \begin{cases} N_C + 1 & if\ I_{sample} \geqslant 1 \\ N_C & if\ I_{sample} < 1 \end{cases} \tag{19}$$

When a fault occurs, the count of sampling points is increased to $N_0/2$, the value of N_C will be close to $N_0/2$. Therefore, the fault detection function is defined as

$$F_{\det ection} = \begin{cases} 1 & if\ \frac{2N_C}{N_0} \geqslant 1 \\ 0 & if\ \frac{2N_C}{N_0} < 1 \end{cases} \tag{20}$$

where $F_{detection}$ = 1, indicates that the detected switch experiences an OCF.

Finally we consider the cases when two switches are faulty simultaneously, as listed in TABLE III. Fig. 10 shows the flowchart of the diagnosis method. The method consists of three main steps:

(a) Current sample processing: initially current samples of the three-phase VSI (equ.15) are taken and normalized. Then the starting point of six switches' FDWs are searched by detecting their zero crossing points (equ.16) when the system is running normally and stably. Periodically reset the received samples are crucial samples within the FDWs of six switched by referring to TABLE IV.

(b) Loads estimation: This step detects the magnitudes of FDWs for six switches, these are the middle point of each FDWs current values, for detailed explanation one can refer to Equation (18). Once this is done unbalance parameters $K_{unbalance}$ can be calculated by substituting the magnitude ($I_{m\_T_1}$-$I_{m\_T_6}$) into formula (11). Then, determine whether re-normalization processing is necessary according to $K_{unbalance}$ value. If the value of the $K_{unbalance}$ is greater than threshold, re-normalization is not required, and if the the value of the $K_{unbalance}$ is lower than threshold, oparate the re-normalization processing by equation (15).

(c) Fault detection: Use formula (19) to statistically calculate the faulty current value number (ratio lower than 1/3) of the FDWs samples. The faulty counting number N_C is obtained and substituted into the fault detection function (equ.20) to obtain the decision of fault result. Finally, check whether this fault detection result is three switches OCF caused by other dual-switch faults as indicated in TABLE III. If not, the diagnosis of the fault occurring in the corresponding switch is established. If yes, the fault result is deemed invalid.

Taking into account the time for clearing the misdiagnosis fault result, it is beneficial to enhance the robustness of the proposed method by setting the last and definitive result of the fault diagnosis if the fault detection persists for two cycles.

V. SIMULATION

To validate the OCF detection method, the MATLAB Simulink package is used, and the simulated inverter driven system is an air-conditioner used in a 25 Tonne train.

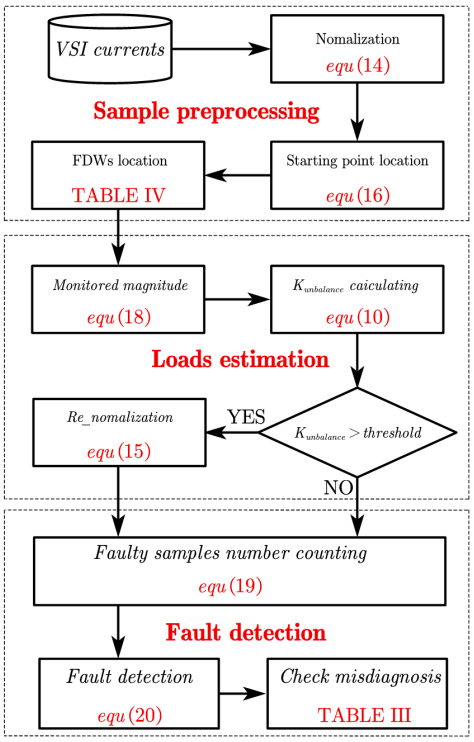

Fig. 10. Flowchart of fault diagnosis method

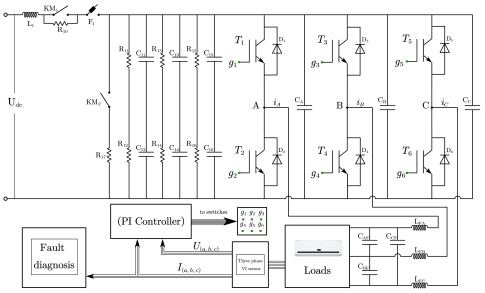

Fig. 11. Air-conditioning inverter schematic for a 25T train

Fig. 11 illustrates the schematic of the inverter system.L_1, R_{10}, KM_1 and F_1 are components of the DC-source side switch snubber circuit, while KM_2 and R_{17} form the discharge circuit for releasing stored energy in the supporting capacitor after the inverter stops. The DC-side support capacitor comprises C_{11}-R_{16} and resistors R_{11}-R_{16}. T_1-T_6 represent the IGBTs (Insulated Gate Bipolar Transistors), D_1-D_6 are the freewheeling diodes for their corresponding switches. The inverter output terminals to the load have L-C filters which are denoted as L_{AF}-C_{AF}, L_{BF}-C_{BF}, and L_{CF}-C_{CF} respectively. Additionally, there are capacitors labeled as C_A, C_B, and C_C for eliminating DC-bus voltage ripples. A PI current controller is used with hysteresis for each phase. The main simulation parameters are provided in TABLE V.

Fig. 12 shows four different cases of OCFs which all have switch T_1 being faulty. Fig. 12(a) is a single T_1 OCF, the FDW for T_1 is located in the positive half wave of phase A. The starting point of the FDW is 0.180s, and the time instance for FDW peak value is 0.182s. The end of FDW is at 0.190s.

TABLE V
MAIN PARAMETERS OF THE EXPERIMENTAL SETUP

Parameters	Value
DC voltage	600V
AC voltage	380V
Frequency of current	50 Hz
Switching frequency	3khz
Suport resistor R(11-16)	33kΩ
Suport capacitor C(11-16)	6.8mF
Filter inductors L(AF,BF,CF)	4.5mH
Filter capacitors C(AF,BF,CF)	90nF
Capacitors C(A,B,C)	1.2nF
Active power	35kw
Reactive power	16.9kw

The current values within the FDW are all bellow 1/3, so the OCF is confirmed. The time duration for detecting this fault is about 8ms.

Figs. 12(b)and(c) show the FDW for T_1&T_2 simultaneously. This is the case when two faulty switches are in the same phase leg. Fig. 12(b) locates T_1 FDW from 0.18s to 0.19s, and its peak value occurs at 0.182s, again it takes 8ms to detect this OCF. For T_2 , Fig 12 (c) locates the FDW from 0.19s to 0.2s in phase A. At the end of FDW, the current values within the FDW are all bellow 1/3 , the time for T_2 fault detected is 18ms.

Figs. 12(d),(e) show T_1&T_4 having OCFs, this is the case when faulty switches are at different phases and different side of inverter simultaneously. The time for both switches having OCF was 0.182s. Fig.12 (d) located T_1 FDW from 0.18s to 0.19s in phase B, it took 8ms to detect the T_1 OCF. For T_4, Fig 12 (e) locates T_4 FDW from 0.196s to 0.206s in phase B, the current values within the FDW are all bellow 1/3, at the end of FDW the OCF of T_4 was detected. The time for fault to be detected is 24ms.

Fig. 12(f),(g)and(h) show both T_1&T_3 having OCF, hence is the case of two faulty switches in the same phase on the different side of inverter. The occurrence for OCF on both switches was 0.182s. Fig 12(f) shows T_1 FDW from 0.18s to 0.19s in phase A, it takes 8ms to detect the T_1 having OCF. For T_3 , Fig 12(c) locates FDW from 0.186s to 0.196s in phase B, the current values within the FDW are all bellow 1/3 , at the end of FDW, the OCF of T_3 is detected. The time taken for detecting this fault is 14ms.

Note that in this case T_6 is also affected by OCF on T_1&T_3. Fig. 12(h) shows that FDW of T_6 from 0.183s to 0193s. At the time instant 0.196s the detection algorithm obtains the result that there are 3 switches in OCF condition. According to TABLE IV, we exclude the assumption that an OCF occurs in T_6 and obtained the result that only T_1 and T_3 having OCFs.

From above simulation results we can conclude that the proposed detection method is capable to diagnose inverter switch OCFs and the time taken for diagnosis is less than 2 fundamental sinusoidal period.

To test the method for diagnosing OCFs under minor unbalanced loads, the simulation is set to emulate the condition of circuit aging hence the phase A impedance becomes higher than normal, leading to a lower phase current. In this case

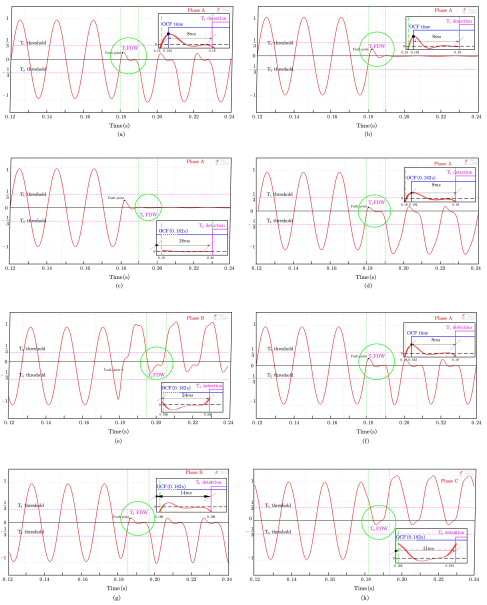

Fig. 12. Fault diagnosis simulation for T_1 OCF in balance loads

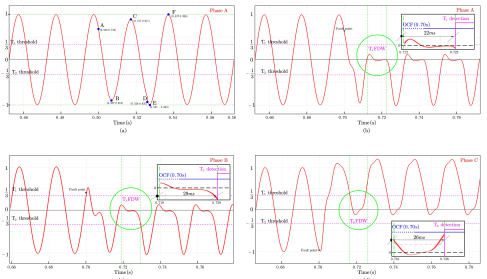

Fig. 13. Fault diagnosis simulation for T_1&T_3 OCFs in unbalance loads

assuming T_1 and T_3 have OCFs simultaneously, making the operation under the most complicated condition.

Fig. 13(b),(c)and(d) show the diagnosis of T_1 and T_3 OCFs. Fig. 13(b) shows that the current values were all below 1/3 with the FDW of T_1. The fault detection time is 22ms. Fig. 13(c) shows that the current values were all below 1/3 with FDW of T_3. The fault detection time is 29ms. Fig. 13(d) shows that the current values were all below 1/3 with the FDW of T_6. The fault detection time is 26ms. So the whole detection time is 29ms and according to the TABLE III, the detection result is T_1&T_3 OCFs and the detection is workable for minor unbalance loads.

Fig. 14 shows the T_1&T_3 OCFs simultaneously. Fig. 14(a) shows the loads power drops significantly at 0.50s (point A), the magnitude $I_{m\_T_1}$ becomes 0.331 (point B) and $I_{m\_T_2}$ becomes 0.330 (point C). The diagnosis model monitors the changes and makes a re-nomalization at point D, the magnitude $I_{m_T_1}$and $I_{m\_T_2}$ all become 1 which can be seen from point E, F.

Fig. 14(b),(c)and(d) show the diagnosis of T_1 and T_3 OCFs. Fig. 14(b) shows that the current values were all below 1/3 with the FDW of T_1. The fault detection time is 12ms. Fig. 14(c) shows that the current values were all below 1/3 with the FDW of T_3. The fault detection time is 18ms. Fig. 14(d)

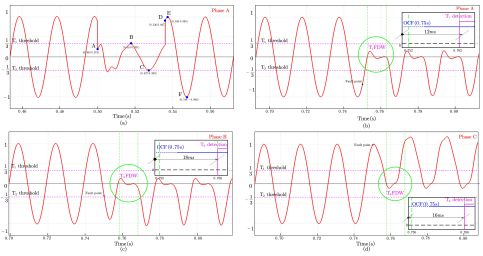

Fig. 14. Fault diagnosis simulation for T_1&T_3 OCFs when loads change rapidly

TABLE VI
MAIN PARAMETERS OF THE EXPERIMENTAL SETUP.

Parameters	Symbol	Value
DC link voltage	V_{dc}	500v
Filter inductances	$L_aL_bL_c$	1.1mH
Filter Capacitors	$C_aC_bC_c$	50uF
Sample period	T_{sample}	5ms
Motor Rated power	U_{RMS}	7.5kW
Motor voltage (fundamental RMS)	U_{RMS}	380V
Motor current (fundamental RMS)	I_{RMS}	15.4A
Rated speed	n	1460rpm(continues)
Power factor	$cos\varphi$	0.86
Rated frequency	f	50.0Hz
Rated torque	T_e	48.96Nm
Efficiency (sine wave power supply)	η	0.93
Motor poles	p	4

shows that the current values were all below 1/3 with the FDW of T_6.The fault detection time is 16ms.So the whole detection time is 18ms and according to the exclusion rule of TABLE III, the detection result is T_1 and T_3 OCFs and the detection method is suitable for the loads rapidly change situation.

VI. EXPERIMENT VERIFICATION

A. Result Analysis

An experimental platform, as shown in Fig. 15, has been established to validate the proposed fault diagnosis method. The setup includes an IGBT three-phase inverter cabinet, associated hardware equipment, a dSPACE system (comprising DS1007, DS2002A/D Board, DS4004I/O Board), and software tools for control, communication, and fault diagnosis algorithm model. The inverter cabinet contains power devices, current sensors, and interfaces with the dSPACE system for real-time communication. The dSPACE Control Desk software allows for real-time monitoring of collected signals and parameter adjustments. The main parameters of the inverter drive system are provided in TABLE VI.

1) Normal Operation at Rated Load: Fig. 16 illustrates the experimental results of a three-phase inverter subjected to four distinct types of fault for T_1. In Fig. 16 (a), depicts a single T_1 OCF (CASE I), with a diagnostic response obtained at 10ms after the fault occurrence. OCFs occurring on T_1 and T_2, (CASE II), are presented in Fig. 16(b)and(c). The diagnosis for T_1 is observed at 18.3ms after the fault, while the diagnosis for T_2 is detected at 28.2ms after the fault

Fig. 15. Experimental setup

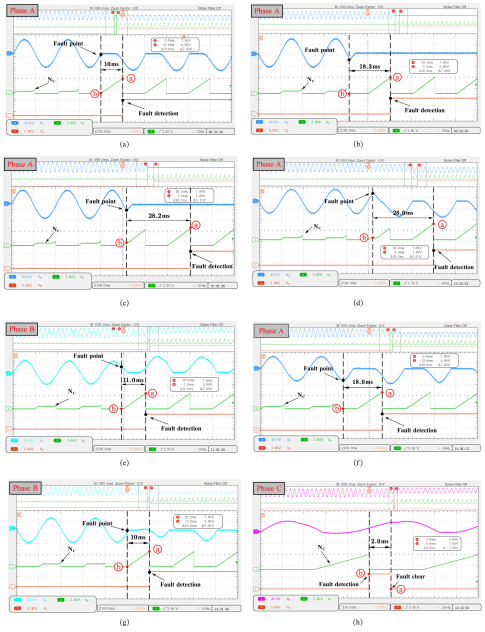

Fig. 16. Experimental results in rated loads

in Fig. 16(b)and(c) respectively. Fig.16(d)and(e) showcase T_1 and T_4, respectively, representing fault occurrences in different phases and sides of the inverter (CASE III). The detection of T_1 fault occurs 28ms after the fault in Fig. 16(d), while in Fig. 16(e), T_1 fault detection happens at 11.0ms after the fault. Furthermore, Fig. 16(f),(g)and(h) exhibit the OCFs of T_1 and T_3, representing a double fault in different phases but on the same side of the inverter (CASE IV). The detection of T_1 fault occurs 18.0ms after the fault in Fig. 16(f), T_3 fault detection happens 10ms after the fault in Fig. 16(g). Fig. 16(g)(h) illustrates the false detection of T_6 fault followed by a clear signal 2.0ms later.

2) VSI operation with unbalance loads: In order to evaluate the performance of the proposed fault diagnosis method under

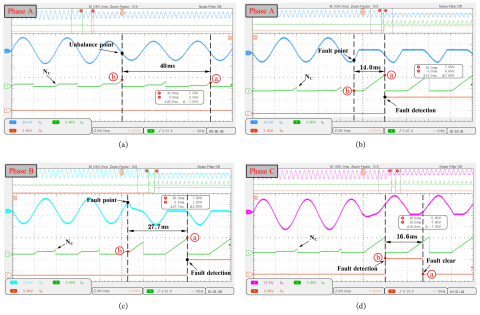

Fig. 17. Experimental results with light unbalance loads

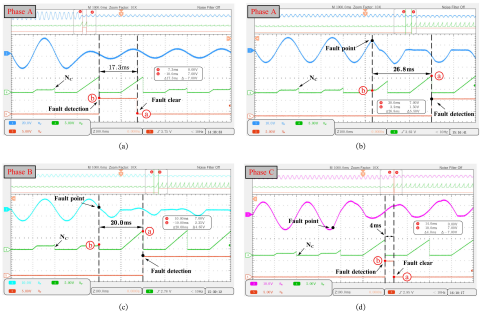

Fig. 18. Experimental results with rapid changing loads

light unbalanced load conditions. The most complex fault scenario (CASE IV) was examined. This scenario involves OCFs of T_1 and T_3 occurring in different phases but on the same side of the inverter. Fig. 17(a) illustrates the variation of the number counting (N_C) of T_1 after the occurrence of light load unbalanced conditions. Following re-normalization, the N_C value remains consistent with the value observed under balanced conditions. Fig. 17(b) shows the detection of the fault at 14.0ms after the occurrence of T_1 OCF. Fig. 17 (c) demonstrates the fault detection at 27.7ms after the occurrence of T_1 OCF. Fig. 17(d) displays the misdiagnosis of T_6 fault followed by a clear signal at 16.6ms later.

3) VSI operation with rapid changing loads: Experimental test was conducted to validate the application of the proposed fault diagnosis method under rapidly changing load conditions. Specifically, the most complex fault scenario (CASE IV) was investigated, involving OCFs of T_1 and T_3 occurring in different phases but on the same side of the inverter. Fig. 18(a) illustrates the variation of the number counting (N_C) of T_1 following intense load fluctuations. Initially, a sudden decrease in current values led to a misdiagnosis for T_1. However, after re-normalization, the fault result cleared after 17.3ms, and the N_C value remained consistent with the rated conditions. Fig. 18(b) demonstrates the detection of the fault 26.8ms after the occurrence of T_1 OCF. Fig. 18(c) displays the fault detection 20.0ms after the occurrence of T_3 OCF. Fig. 18(d) reveals the misdiagnosis of T_6 fault followed by a clear signal 4.0ms later. The experimental results demonstrate that the proposed fault diagnosis method achieves rapid diagnosis and localization of switch OCFs in a three-phase voltage source inverter (VSI). Furthermore, the method exhibits robustness to different load conditions.

B. Comparison Between the fault diagnosis Method

TABLE V summarizes the characteristics of fault diagnosis methods for three-phase inverters. The table provides a comprehensive analysis of fault diagnosis time, types of faults identified, computational requirements, adaptability to load variations, and robustness. The characteristics of the proposed fault diagnosis method in this paper are listed at the bottom of the table. Voltage-based methods [18], [19], [20], [21]. These methods have low computational requirements. However, due to the high complexity of voltage for double switch open-circuit faults (OCFs), the fault types addressed in [18] and [21] are limited to single switch OCFs. Additionally, these methods exhibit weak adaptability to load variations. Current-based methods [22], [23], [24] can achieve fault diagnosis within a shorter time frame. However, these three methods exhibit poor robustness due to strong dependence on the standard current model. Method [26] demonstrates good robustness but sacrifices diagnosis time, resulting in a longer diagnosis time of up to 1.3s. Model-based methods [27], [28], [29], these methods offer fast diagnostic capabilities but require meticulous handling of the constructed model, thus demanding computational support. They exhibit moderate adaptability to load variations and robustness, making them a balanced diagnostic approach. Intelligent technology-based methods [30], [31], [32] leverage intelligent technologies such as neural networks for fault diagnosis through feature extraction. On one hand, implementing intelligent technologies requires high equipment requirements and high computational support. On the other hand, the current methods lack sufficient consideration for load variations, and the establishment of databases relies on simulation. However, they hold potential for improved robustness. In comparison to these methods, the proposed fault diagnosis method in this paper demonstrates rapid fault detection and location, achieving it within 0.04s (two fundamental circles). It can efficiently handle load variations, including unbalanced load states and abrupt load changes. The method required data processing is straightforward, with low computational requirements, making it highly implementable. After addressing misdiagnosis issues, the method exhibits excellent robustness.

VII. CONCLUSION

This paper has developed a current analysis method for three-phase voltage source inverters (VSIs) having switch open-circuit faults (OCFs). The method could identify the abnormal patterns of the current waves, known as fault detection waveforms, due to the switch OCFs, promptly. The continuously analyzing the FDW starting and peak values greatly enhances the robustness of current-based fault diagnosis for three-phase VSIs. Furthermore, the incorporation of a unbalance ratio judgment and re-normalization in the method enabled it to handle complex load variations during fault diagnosis. The technique has demonstrated its capability to function desirably during the light load imbalance and sudden load changing conditions. The effectiveness of the proposed method has been validated through both simulation and real experimental tests. The results has shown that the proposed fault diagnosis method can quickly and accurately

TABLE VII
COMPARISON WITH OTHER FAULT DIAGNOSIS METHODS

Ref	Diagnosis method	Diagnosis time	Faults types	Calculation burden	Loads adaptability	Robustness
(18)	Voltage based	/	6	low	high	high
(19)	Voltage based	0.02s	21	low	low	low
(20)	Voltage based	0.04s	21	low	low	low
(21)	Voltage based	/	6	low	low	low
(22)	Current based	0.07s	21	low	low	moderate
(23)	Current based	/	12	low	low	low
(24)	Current based	0.04s	21	low	moderate	moderate
(25)	Current based	1.30s	21	moderate	/	high
(26)	Current based	0.002s	6	low	low	low
(27)	Model based	0.04s	21	moderate	low	moderate
(28)	Model based	0.01s	6	moderate	low	low
(29)	Model based	0.01s	/	moderate	low	moderate
(30)	Intelligent technologies	/	6	high	moderate	moderate
(31)	Intelligent technologies	0.06s	/	high	moderate	moderate
(32)	Intelligent technologies	/	/	high	moderate	high
This paper	The proposed method	0.04s	21	low	high	high

diagnose single switch and double switch open-circuit faults in three-phase VSIs. The diagnostic results for faults under load changes and load imbalance conditions highlight the method's high robustness in handling load variations.

REFERENCES

[1] M. R. Miveh, M. F. Rahmat, A. A. Ghadimi, and M. W. Mustafa, "Control techniques for three-phase four-leg voltage source inverters in autonomous microgrids: A review," *Renewable and Sustainable Energy Reviews*, vol. 54, pp. 1592–1610, 2016.

[2] H. Chen and H. Zhao, "Review on pulse-width modulation strategies for common-mode voltage reduction in three-phase voltage-source inverters," *IET Power Electronics*, vol. 9, no. 14, pp. 2611–2620, 2016.

[3] J. Chen, D. Sha, J. Zhang, and X. Liao, "An sic mosfet based three-phase zvs inverter employing variable switching frequency space vector pwm control," *IEEE Transactions on Power Electronics*, vol. 34, no. 7, pp. 6320–6331, 2018.

[4] Y. Wang, Z. Li, M. Xu, and H. Ma, "A comparative study of two diagnostic methods based on the switching voltage pattern for igbt open-circuit faults in voltage-source inverters," *Journal of Power Electronics*, vol. 16, no. 3, pp. 1087–1096, 2016.

[5] J. Xu, J. Han, Y. Wang, M. Ali, and H. Tang, "High-frequency sic three-phase vsis with common-mode voltage reduction and improved performance using novel tri-state pwm method," *IEEE Transactions on Power Electronics*, vol. 34, no. 2, pp. 1809–1822, 2018.

[6] H. Yuruk, O. Keysan, and B. Ulutas, "Comparison of the effects of non-linearities for si mosfet and gan e-hemt based vsis," *IEEE Transactions on Industrial Electronics*, vol. 68, no. 7, pp. 5606–5615, 2020.

[7] S. Karimi, P. Poure, and S. Saadate, "Fast power switch failure detection for fault tolerant voltage source inverters using fpga," *IET power electronics*, vol. 2, no. 4, pp. 346–354, 2009.

[8] S. Kwak and J.-C. Park, "Predictive control method with future zero-sequence voltage to reduce switching losses in three-phase voltage source inverters," *IEEE Transactions on Power Electronics*, vol. 30, no. 3, pp. 1558–1566, 2014.

[9] M. Yaghoubi, J. S. Moghani, N. Noroozi, and M. R. Zolghadri, "Igbt open-circuit fault diagnosis in a quasi-z-source inverter," *IEEE Transactions on Industrial Electronics*, vol. 66, no. 4, pp. 2847–2856, 2018.

[10] O. Dieterle, T. Greiner, and P. Heidrich, "Control of a pmsm with quadruple three-phase star-connected windings under inverter short-circuit fault," *IEEE Transactions on Industrial Electronics*, vol. 66, no. 1, pp. 685–695, 2018.

[11] D. Espinoza-Trejo, D. Campos-Delgado, E. Barcenas, and F. Martınez-Lopez, "Robust fault diagnosis scheme for open-circuit faults in voltage source inverters feeding induction motors by using non-linear proportional-integral observers," *IET Power Electronics*, vol. 5, no. 7, pp. 1204–1216, 2012.

[12] I. Jlassi, J. O. Estima, S. K. El Khil, N. M. Bellaaj, and A. J. M. Cardoso, "A robust observer-based method for igbts and current sensors fault diagnosis in voltage-source inverters of pmsm drives," *IEEE Transactions on Industry Applications*, vol. 53, no. 3, pp. 2894–2905, 2016.

[13] F. Wu, Y. Hao, J. Zhao, and Y. Liu, "Current similarity based open-circuit fault diagnosis for induction motor drives with discrete wavelet transform," *Microelectronics Reliability*, vol. 75, pp. 309–316, 2017.

[14] S. Lee, F. Chen, T. M. Jahns, and B. Sarlioglu, "Review on switching device fault, protection, and fault-tolerant topologies of current source inverter," in *2021 IEEE 13th International Symposium on Diagnostics for Electrical Machines, Power Electronics and Drives (SDEMPED)*, vol. 1, pp. 489–495, IEEE, 2021.

[15] M. T. Fard, J. He, and Z. Wang, "Fault diagnosis and fault-tolerant operation of current source inverter for safety-critical applications," in *2020 IEEE Transportation Electrification Conference & Expo (ITEC)*, pp. 925–929, IEEE, 2020.

[16] B. Jiang and Q. An, "A novel diagnostic technique for open-switch faults of inverters based on operating mode analysis," in *Zhongguo Dianji Gongcheng Xuebao(Proceedings of the Chinese Society of Electrical Engineering)*, vol. 32, pp. 30–37, Chinese Society for Electrical Engineering, 2012.

[17] Q. Wang, Y. Wang, Z. Zhang, and Z. Song, "A diagnosis method for inverter open-circuit faults of brushless dc motor driver systems," *Proc. CSEE*, vol. 33, no. 24, pp. 114–122, 2013.

[18] C. Shu, C. Ya-Ting, Y. Tian-Jian, and W. Xun, "A novel diagnostic technique for open-circuited faults of inverters based on output line-to-line voltage model," *IEEE Transactions on Industrial Electronics*, vol. 63, no. 7, pp. 4412–4421, 2016.

[19] X. Wu, T.-F. Chen, S. Cheng, T. Yu, C. Xiang, and K. Li, "A noninvasive and robust diagnostic method for open-circuit faults of three-level inverters," *IEEE Access*, vol. 7, pp. 2006–2016, 2018.

[20] X. Xu and F. Yu, "A switch open-circuit fault diagnosis method for three-phase inverters based on voltage patterns," in *2022 2nd International Conference on Electrical Engineering and Control Science (IC2ECS)*, pp. 901–908, IEEE, 2022.

[21] Y. Li, X. Cheng, Z. Yang, Z. Huang, and M. Ke, "Inverter fault diagnosis algorithm based on midpoint voltage deviation polarity and topology reconstruction," in *2023 IEEE 3rd International Conference on Power, Electronics and Computer Applications (ICPECA)*, pp. 62–67, IEEE, 2023.

[22] H. Yan, Y. Xu, J. Zou, Y. Fang, and F. Cai, "A novel open-circuit fault diagnosis method for voltage source inverters with a single current sensor," *IEEE Transactions on Power Electronics*, vol. 33, no. 10, pp. 8775–8786, 2017.

[23] Z. Jian-Jian, C. Yong, C. Zhang-Yong, and Z. Anjian, "Open-switch fault diagnosis method in voltage-source inverters based on phase currents," *IEEE access*, vol. 7, pp. 63619–63625, 2019.

[24] K. Li, S. Cheng, T. Yu, X. Wu, C. Xiang, and A. Bilal, "An on-line multiple open-circuit fault diagnostic technique for railway vehicle air-conditioning inverters," *IEEE Transactions on Vehicular Technology*, vol. 69, no. 7, pp. 7026–7039, 2020.

[25] Y. Zhou, J. Zhao, Y. Song, J. Sun, H. Fu, and M. Chu, "A seasonal–trend-decomposition-based voltage-source-inverter open-circuit fault diagnosis method," *IEEE Transactions on Power Electronics*, vol. 37, no. 12, pp. 15517–15527, 2022.

[26] Z. Li, P. Wheeler, A. Watson, A. Costabeber, B. Wang, Y. Ren, Z. Bai, and H. Ma, "A fast diagnosis method for both igbt faults and current

sensor faults in grid-tied three-phase inverters with two current sensors," *IEEE Transactions on Power Electronics*, vol. 35, no. 5, pp. 5267–5278, 2019.
[27] Z. Li, H. Ma, Z. Bai, Y. Wang, and B. Wang, "Fast transistor open-circuit faults diagnosis in grid-tied three-phase vsis based on average bridge arm pole-to-pole voltages and error-adaptive thresholds," *IEEE Transactions on Power Electronics*, vol. 33, no. 9, pp. 8040–8051, 2017.
[28] Z. Huang and Z. Wang, "A fault diagnosis algorithm for microgrid three-phase inverter based on trend relationship of adjacent fold lines," *IEEE Transactions on Industrial Informatics*, vol. 16, no. 1, pp. 267–276, 2019.
[29] W. Zhang and Y. He, "A hypothesis method for t-type three-level inverters open-circuit fault diagnosis based on output phase voltage model," *IEEE Transactions on Power Electronics*, vol. 37, no. 8, pp. 9718–9732, 2022.
[30] S. Zhang, R. Wang, Y. Si, and L. Wang, "An improved convolutional neural network for three-phase inverter fault diagnosis," *IEEE Transactions on Instrumentation and Measurement*, vol. 71, pp. 1–15, 2021.
[31] Y. Xia and Y. Xu, "A transferrable data-driven method for igbt open-circuit fault diagnosis in three-phase inverters," *IEEE Transactions on Power Electronics*, vol. 36, no. 12, pp. 13478–13488, 2021.
[32] Y. Si, R. Wang, S. Zhang, W. Zhou, A. Lin, and Y. Wang, "fault diagnosis based on attention collaborative lstm networks for npc three-level inverters," *IEEE Transactions on Instrumentation and Measurement*, vol. 71, pp. 1–16, 2022.

Yu Luo received the B.E. degree in electrical automation from Changsha University of Science and Technology, China, in 2013. Then received the M.S. degree electrical engineering from Changsha University of Science and Technology, China, in 2016. He is currently studying PhD degree at School of Transportation Engineering, Central South University, China.His research interests include fault diagnosis and fault tolerant control of power electronic converters, train control and traction electric drive.

Li Zhang (M'03-SM'10)received the PhD degree and was a research fellow in Oxford University,UK.She was then a lecturer at the University of Bradford and is currently a senior lecturer in the School of Electronic and Electrical Engineering at the University of Leeds,UK.Dr Li Zhang is an adjunct professor in Chongqing University, China from 2006 till now and Joint Grant holder of China State Natural Science Foundation Fund(60712,201401-2017 12)entitled:Analysis and research on the hot spot effect and it's control method of photovoltaic system.She is an associate editor for IEEE,Transaction on Power Electronics and has also been the associate editor of IET proceedings on Power Electronics between 2014 to 2017.She has authored and co-authored three books on power converter circuits and wind power electricity generation.She has authored and co-authored more than 130 technical papers in the fields of power electronics,renewable power generation system and wind generator control.

Chunyang Chen was born in Nanling, China, in 1962. He received the B.E. degree in electric locomotive from Southwest Jiaotong University, Master degree from Hunan University, and Ph.D degree from Beijing Jiaotong University. He used to be the deputy director of Science and Technology Department of the Ministry of Railways, and the president of Southwest Jiaotong University. Now, he serves as the vice president of Central South University. His research interests include the electric locomotive and intelligent transportation system.

Kang Li (M'05–SM'11) received B.Sc. degree in Industrial Automation from Xiangtan University, Hunan, China, in 1989, M.Sc. degree in Control Theory and Applications from Harbin Institute of Technology, Harbin, China, in 1992, and Ph.D. degree in Control Theory and Applications from Shanghai Jiaotong University, Shanghai, China, in 1995. He also received D.Sc. degree in Engineering from Queen's University Belfast, UK, in 2015. He currently holds the Chair of Smart Energy Systems at the University of Leeds, UK. His research interests cover nonlinear system modelling, identification, and control, and machine learning, with substantial applications to energy and power systems, transport decarbonization, and energy management in energy intensive manufacturing processes.

Kaidi Li was born in Nanning, China, 1992. He received the B.E. degree in electrical engineering from Changsha University of Science and Technology, China, in 2013. Then received the M.S. degree electrical engineering from the Central South University (CSU), China, in 2016, and the Ph.D. degree in traffic equipment and information engineering from CSU, in 2019. He is currently working in Shenzhen Metro Group Co., Ltd., Shenzhen, China.

His research areas include fault diagnosis and fault tolerant control of power electronic converters.